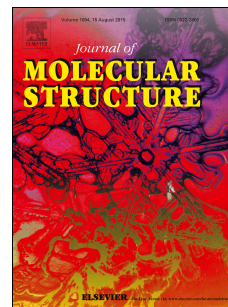


# Journal Pre-proof

3 $\beta$ -acetoxy cholest-5-ene crystals: Catalytic synthesis, structural elucidation, contribution of intermolecular interactions and density functional theory calculations

Ashraf Mashrai, Mohammad Jane Alam, Bushra Amer, Musheer Ahmed, Shabbir Ahmad



PII: S0022-2860(20)31158-3

DOI: <https://doi.org/10.1016/j.molstruc.2020.128833>

Reference: MOLSTR 128833

To appear in: *Journal of Molecular Structure*

Received Date: 20 May 2020

Revised Date: 27 June 2020

Accepted Date: 3 July 2020

Please cite this article as: A. Mashrai, M.J. Alam, B. Amer, M. Ahmed, S. Ahmad, 3 $\beta$ -acetoxy cholest-5-ene crystals: Catalytic synthesis, structural elucidation, contribution of intermolecular interactions and density functional theory calculations, *Journal of Molecular Structure* (2020), doi: <https://doi.org/10.1016/j.molstruc.2020.128833>.

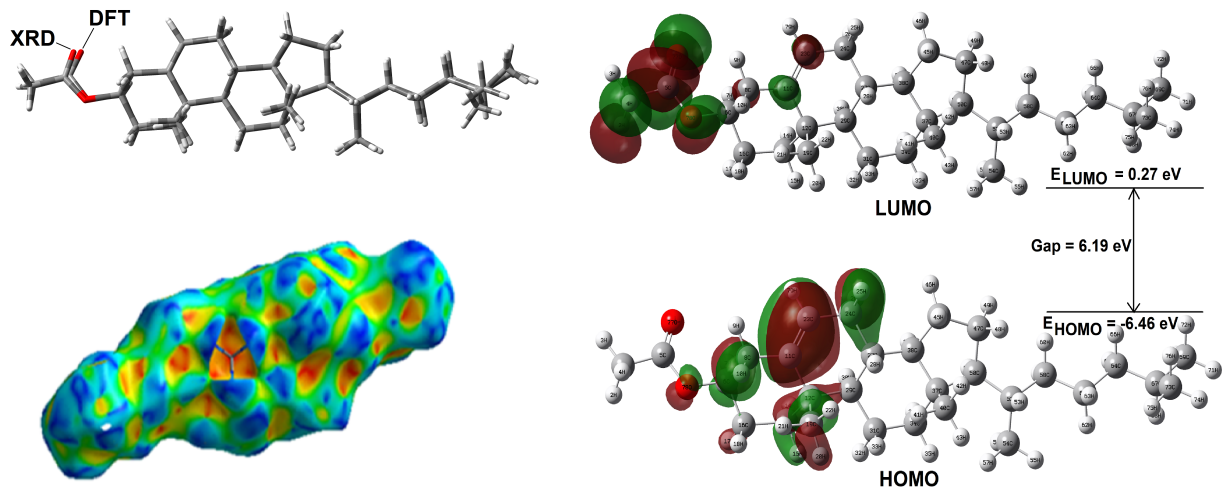
This is a PDF file of an article that has undergone enhancements after acceptance, such as the addition of a cover page and metadata, and formatting for readability, but it is not yet the definitive version of record. This version will undergo additional copyediting, typesetting and review before it is published in its final form, but we are providing this version to give early visibility of the article. Please note that, during the production process, errors may be discovered which could affect the content, and all legal disclaimers that apply to the journal pertain.

© 2020 Published by Elsevier B.V.

**Credit Author Statement:**

The contribution(s) of all authors is stated using relevant categories.

- Ashraf Mashrai: Conceptualization, Synthesis of the compound, Crystallization, Writing-Original draft preparation.
- Mohammad Jane Alam: DFT calculations, theoretical data visualization, Writing-Original draft preparation.
- Bushra Amer: Characterization of the compound, Writing-Original draft preparation.
- Musheer Ahmed: Single crystal XRD characterization and structure solution.
- Shabbir Ahmad: Supervision, Software.



Journal Pre-proof

### **3 $\beta$ -Acetoxy cholest-5-ene crystals: Catalytic synthesis, structural elucidation, contribution of intermolecular interactions and density functional theory calculations**

Ashraf Mashrai<sup>a</sup>, Mohammad Jane Alam<sup>\*b</sup>, Bushra Amer<sup>c</sup>, Musheer Ahmed<sup>d</sup>, Shabbir Ahmad<sup>b</sup>

<sup>a</sup>*Department of Pharmacy, University of Science and Technology, Ibb Branch, Yemen*

<sup>b</sup>*Department of Chemistry, Aligarh Muslim University, Aligarh 202002, India*

<sup>b</sup>*Department of Physics, Aligarh Muslim University, Aligarh 202002, India*

<sup>c</sup>*Faculty of Medicine and Health Sciences, Sana'a University, Yemen*

<sup>d</sup>*Department of Applied Chemistry, Aligarh Muslim University, Aligarh 202002, India*

#### **ABSTRACT**

In this work, we present the synthesis of 3 $\beta$ -acetoxy cholest-5-ene using zinc triflate Zn(OTf)<sub>2</sub> as a catalyst. The synthesized molecule has been characterized by single crystal XRD, spectroscopic techniques and density functional theory (DFT) calculations. The compound crystallizes in the monoclinic space group  $P2_1$  with cell dimensions,  $a = 16.585(2)$  Å,  $b = 9.5175(12)$  Å,  $c = 17.656(2)$  Å,  $\alpha = 90.00$ ,  $\beta = 106.369(4)$ ,  $\gamma = 90.00$ . The systematic analysis of intermolecular interactions in crystal structure was accomplished by Hirshfeld surface analysis and fingerprint plot. Molecules are linked by a combination of C---H, C---C, H---H and O---H contacts, which have clear signatures in the fingerprint plots. The theoretical DFT/B3LYP calculations have been attempted to obtain the optimized geometry, IR/NMR spectra, natural bond orbitals, frontier molecular orbitals and various structure based molecular properties. We compared the conformations of the compound in solid state and in solution by calculation of dihedral angles and coupling constant values.

*Keywords:* 3 $\beta$ -Acetoxy cholest-5-ene; Zinc triflate; Hirshfeld surface; DFT.

---

\*Corresponding author: [janealam.ph@amu.ac.in](mailto:janealam.ph@amu.ac.in) , [mjalamamu@gmail.com](mailto:mjalamamu@gmail.com)

---

## 1. Introduction

Cholesterol cell toxicity is well-known to be influenced by C-3 esterification [1]. The esterification catalyzed through acyl coenzyme A, cholesterol acyl transferase intracellularly or lecithin cholesterol acyl transferase in plasma. Cholesteryl esters have been observed in lipoproteins and oxidised lipoproteins and it shows the way by which the cholesterol can be accrued in cells and lipid droplets. Further, esters can potentially play a role as hydrophilic weak acid transporters to target cancer cells [2]. In the last few decades, much attempt has been devoted to developing transition metal catalyzed for the facile construction of the skeleton of heterocycles [3]. Zinc triflate has been utilized as a catalyst in a comprehensive range of organic syntheses in the past few years [4]. Hirshfeld surface analysis approach is a very convenient and widely used tool in the field of crystallography for the investigation of different kinds of intermolecular interactions and crystal packing. Hirshfeld surface [5-8] based tools seem to be extremely appropriate for the visualization of variations in the intermolecular interactions as crystal structure gives the most obvious insight of the intermolecular contacts and crystal packing. The surfaces encode knowledge about all intermolecular interactions offers a facile way for getting an idea on crystal packing. The associated fingerprint plot [9, 10] investigates quantitatively the varieties of intermolecular contacts experienced by molecules and depicts this valuable information in a suitable color plot. As part of our ongoing studies on crystal analysis of steroidal compounds [11-14], catalytic synthesis, single crystal analysis of  $3\beta$ -acetoxy cholest-5-ene was carried out along with the Hirshfeld surface analysis to explore the close contacts and crystal packing. DFT/B3LYP method is widely used in quantum chemical calculations of molecules due to its low computational cost and good accuracy. This method has been employed on various steroids molecules to obtain their structural information, spectra and physiochemical

properties [15-18]. In the present work, DFT/B3LYP calculation results are used not only to support the experimental data like molecular geometry, FTIR and NMR spectra but also to explore various structure based molecular properties. The optimized geometry and the simulated spectra (IR and NMR) have been compared with the experimental one and they are found in good agreement. Thus, structure based theoretical data like HOMO-LUMO energies, molecular electrostatic potential (MEP), non-linear optical (NLO) parameters, thermodynamic quantities and global reactivity indices of the present compound has been accurately estimated. In addition, spectral, thermal and morphological properties were also investigated.

## 2. Experimental and theoretical details

### 2.1. General

All reagents and solvents were obtained commercially and utilized as received. Kofler apparatus was used to detect the Melting point. The FTIR spectrum of present compound was recorded by KBr pellets technique using Interspec 2020 FT-IR Spectrometer spectro Lab in the region 4000-400  $\text{cm}^{-1}$ . NMR spectra were measured in  $\text{CDCl}_3$  on a Bruker Avance II 400 NMR Spectrometer at 400 MHz ( $^1\text{H}$ -NMR) and 100 MHz ( $^{13}\text{C}$ -NMR). Chemical shifts ( $\delta$  in ppm) are reported relative to the TMS ( $^1\text{H}$  NMR) and to the solvent signal ( $^{13}\text{C}$  NMR spectra). Elemental analyses of the present compound were performed on Perkin Elmer 2400 CHN Elemental Analyzer. Thermal study of the compound was performed using TGA/DTA-60H instrument (SHIMADZU) at a heating rate of 20  $^\circ\text{C min}^{-1}$  from ambient temperature to 800 $^\circ\text{C}$ . Powder X-ray diffraction ( $\text{CuK}\alpha$  radiation, scan rate 3 $^\circ/\text{min}$ , 293 K,  $\lambda = 1.54\text{\AA}$ ) was performed on a Bruker D8 Advance Series 2 powder X-ray diffractometer. Mass spectra were measured on a JEOL D-300 Mass Spectrometer. The surface morphology of the compound was monitored using JEOL JSM-6510LV scanning electron microscope (SEM), Thin layer chromatography (TLC) plates coated

with silica gel G were exposed to iodine vapors to see the homogeneity as well as the progress of reaction. Sodium sulfate in anhydrous form was used as a drying agent.

### 2.2. Synthesis 3 $\beta$ -acetoxy cholest-5-ene

To a mixture of cholesterol (1 mmol) and acetic anhydride (1 mmol) in methylene chloride (20 mL), Zn(OTf)<sub>2</sub> (0.1 mol %) was added. This mixture was stirred at room temperature for 30 min. Completion of reaction was monitored by TLC, after quenching with added sat. NaHCO<sub>3</sub> aq the products extracted into methylene chloride (3 $\times$ 20 mL). The organic layer after the washing with water, dried over anhydrous Na<sub>2</sub>SO<sub>4</sub> and concentrated to obtain the desirable product [19]. The compound was crystallized from acetone and obtained colorless crystals appropriate for X-ray diffraction. Yield (91%); m.p. 112 °C; Anal. Calc. for C<sub>29</sub>H<sub>48</sub>O<sub>2</sub>: C, 81.25; H, 11.29 (%). Found: C, 81.29; H, 11.26 (%); IR (KBr, cm<sup>-1</sup>): 2948, 2870 (C-H, stretching), 1736 (C=O), 1465, 1368 (C-H, bending), 1670 (C=C), 1246 (C-O); <sup>1</sup>H NMR (CDCl<sub>3</sub>, 400 MHz):  $\delta$  5.4 (1H, t, C10H,  $J$  = 2.31, 2.78 Hz), 4.54 (1H, m, C3 $\alpha$ -H,  $W_{1/2}$  = 14 Hz, axial), 2.01 (3H, s, OCOCH<sub>3</sub>), 1.10 (3H, s, 8-CH<sub>3</sub>) 0.67 (3H, s, 16-CH<sub>3</sub>), 0.90 and 0.85 (other methyl protons); <sup>13</sup>C NMR (CDCl<sub>3</sub>, 100 MHz):  $\delta$  170.19 (C=O), 139.54 (C-5), 122.57 (C-10), 77.43 (C-O), 56.67, 56.17, 50.03, 42.28, 39.73, 39.52, 38.11, 37, 36.53, 36.21, 35.81, 31.88, 31.84, 28.24, 27.98, 27.76, 24.27, 23.89, 22.82, 22.58, 21.23, 21.03, 19.28, 18.72, 11.84; MS (ESI): m/z 428.37 [M<sup>+</sup>].

### 2.3. X-ray diffraction

The intensity data (three dimensional) for the titled compound were generated at 100 K on Bruker KAPPA APEXII DUO diffractometer using Cu K $\alpha$  radiation ( $\lambda$ = 1.54178 Å). The structure was solved by direct methods using SHELXS-97 software (SHELDRICK, 1990). Isotropic refinement of the structure by least-squares methods was carried out by using

SHELXL-97 (SHELDRICK, 1997) followed by anisotropic refinement on  $F^2$  of all the non-hydrogen atoms. Crystallographic data (excluding structure factors) of  $3\beta$ -acetoxy cholest-5-ene reported in present article have been deposited with the Cambridge Crystallographic Data Centre (CCDC) as deposition No. CCDC 1837266. Positions of all hydrogen atoms were obtained geometrically with Uiso (H) = 1.2-1.5 Å<sup>2</sup> Ueq (parent atom). A riding model was utilized in their refinement (C-H = 0.98-1.00 Å).

#### 2.4. Hirshfeld surfaces calculations

Molecular Hirshfeld surfaces [20] in the crystal structure have been generated from electron distribution which was computed as the sum of spherical atom electron densities [21]. Hirshfeld surface is unique for a given crystal structure and set of spherical atomic electron densities [22]. This property suggests the possibility to know additional insight into the intermolecular interaction of molecular crystals. In this work, the Hirshfeld surfaces as well as fingerprint plots were produced using CrystalExplorer [23] with the results of X-ray studies. In the calculations, bond lengths to hydrogen atoms were normalized to typical neutron values (C-H = 1.083 Å) [24] in order to make sure the internal evenness and independence of results from the crystal structure refinement method. The 2D fingerprint plots were presented by using the standard view with the  $d_e$  and  $d_i$  distance scales (0.6-2.6 Å) displayed on the graph axes. The normalized contact distance ( $d_{norm}$ ) related to both  $d_e$ ,  $d_i$  and the  $vdw$  radii of the atom, given in Eq. (1), enables to identify the regions of particular importance for intermolecular interactions [25]

$$d_{norm} = \frac{d_i - r_i^{vdw}}{r_i^{vdw}} + \frac{d_e - r_e^{vdw}}{r_e^{vdw}} \quad (1)$$

Distances  $d_e$  and  $d_i$  in the expression of  $d_{norm}$ , where two Hirshfeld surfaces touch, display a red spot identical in color intensity as well as size/shape because of the symmetry between  $d_e$  and  $d_i$ .

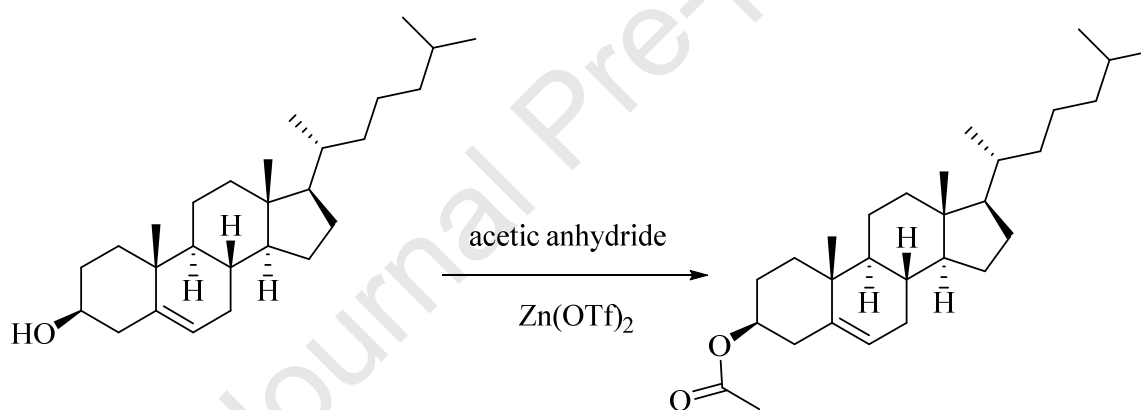
### 2.5. Theoretical calculations

Present theoretical calculations were performed using hybrid functionals (B3LYP) within DFT framework along with basis set 6-311G(d,p) by Gaussian 09 software [26-28]. The initial coordinates of the present geometry were taken from the asymmetric unit of present crystal from crystallographic information file. Potential energy surface scan was performed by varying two dihedral angles i.e. C16-C6-O-C and C6-O-C5-C1 to check stable conformer of the 3 $\beta$ -acetoxy cholest-5-ene. The optimized geometry and vibrational spectra of the title molecule were computed in the ground electronic state at B3LYP/6-311G(d,p) level of theory (in vacuum). The IR bands appeared in the FTIR were assigned with the great accuracy using animated modes visualized by Gauss View 5 program [29]. The theoretical IR spectrum was presented by Lorentzian band shape with FWHM of 5 cm<sup>-1</sup>. In general, harmonic frequencies overestimate the experimental IR frequencies mainly due to excluding anharmonic nature of molecular vibrations in quantum chemical calculations. Therefore, a uniform scaling factor, 0.967, was used to scale down the harmonic frequencies [30]. The NMR spectra (<sup>1</sup>H and <sup>13</sup>C) were simulated in the solution phase (CDCl<sub>3</sub>) using integral equation formalism of polarizable continuum model (IEF-PCM) within GIAO-B3LYP/6-311G(d,p) method. The chemical shifts (in ppm) were calculated with respect to TMS shielding (as reference) at same level of theory. Natural atomic charges, hybridization, and hyper conjugative interactions energies were obtained by natural bond orbital analysis (NBO) using NBO 3.1 program [31]. In addition, molecular energy, dipole moment, frontier molecular orbitals (HOMO-LUMO), non-linear optical (NLO) parameters, molecular

electrostatic potential, thermodynamic data and various reactivity descriptors for the synthesized compound have been also computed at same level of theory.

### 3. Results and discussion

In this work, we synthesized  $3\beta$ -acetoxy cholest-5-ene using  $\text{Zn}(\text{OTf})_2$  as a catalyst instead of using pyridine [32]. Our approach offered the same product in less time and better yield. IR,  $^1\text{H}$  NMR,  $^{13}\text{C}$  NMR, elemental analysis and single crystal XRD data agree with the supposed structure depicted in scheme 1. The DFT/B3LYP results are used to support experimental data for the presented compound.



**Scheme 1:** Synthesis of  $3\beta$ -acetoxy cholest-5-ene from cholesterol.

#### 3.1. Description of crystal structure

The asymmetric unit of  $3\beta$ -acetoxy cholest-5-ene,  $\text{C}_{29}\text{H}_{48}\text{O}_2$ , consists of two crystallographically independent molecules, A and B, while unit cell contains 4 molecules. In both molecules, the three cyclohexane rings are in chair conformations while the cyclopentane rings show envelope and twist conformations in molecules A and B, correspondingly. The synthesized compound crystallizes in the monoclinic system with space group  $P2_1$  due to the presence of 8 *chiral* centers [24]. The molecules are arranged in head to tail manner and the crystal packing is stabilized by a

combination of intermolecular interactions (Fig. 1). The B/C and C/D ring systems are *trans* fused about the C(12)-C(13) and C(16)-C(17) bonds, respectively, while the A/B ring junction is *quasi-trans*. Side-chain is extended with a *gauche-trans* conformation of the terminal C28 and C29 methyl groups (Fig. 1). The bond distances and bond angle in the compound are found to be almost equivalent to earlier report and within normal ranges [33]. At position 3, the acetoxy group is equatorial and antiperiplanar to the C3-C8 bond with torsion angle 177.95 and not involved in any hydrogen bond. The absolute configurations of chiral centres were established from the structure shown, these sites exhibit the following chiralities: C3 = *S*, C6 = *R*, C12 = *S*, C13 = *S*, C16 = *R*, C17 = *S*, C21 = *R* and C22 = *R*. Due to the non-existence of the strong hydrogen bond donor in the crystallize molecule, the cohesion of the crystal structure can only be attributed to van der Waals interactions. Important crystallographic data along with refinement details of the structural analyses are summarized in Table 1. It is important to mention that previous report [34] did not provide any information concerning the intermolecular contacts, however our, study demonstrates the existence of short intermolecular contacts.

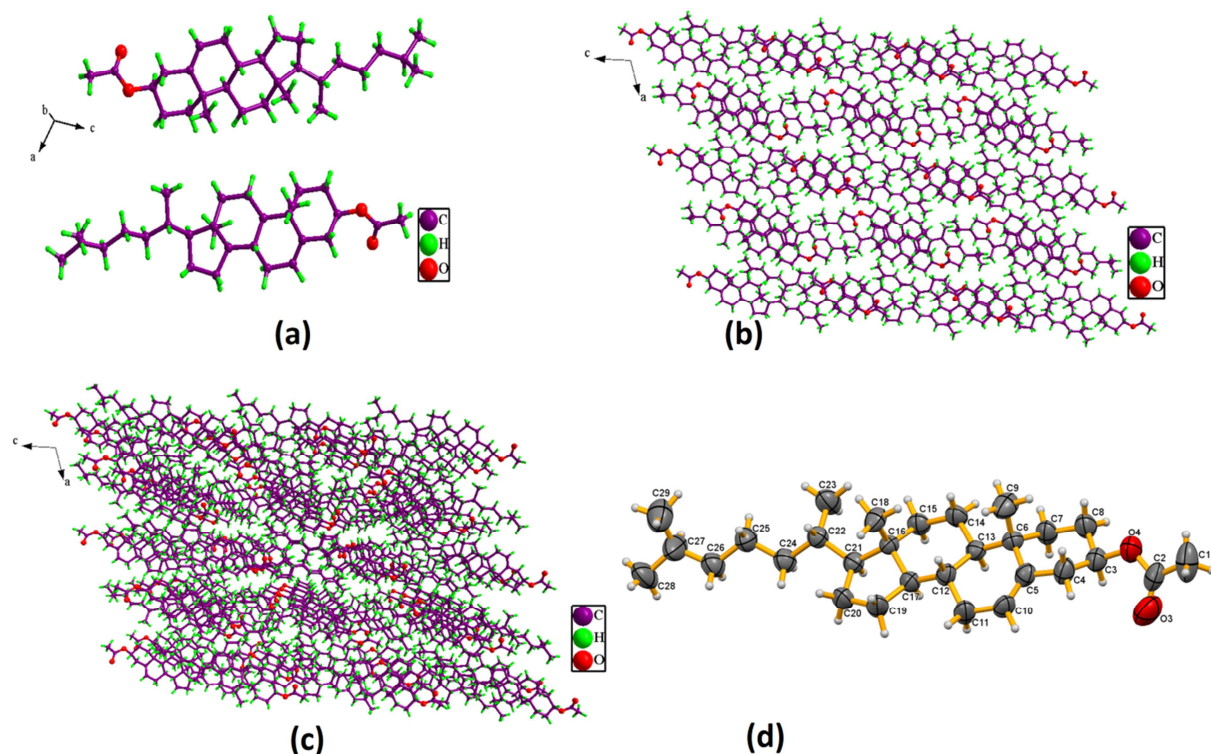


**Fig. 1.** Crystallographic structure of  $3\beta$ -acetoxy cholest-5-ene: (a) asymmetric unit (b) 2D-view (c) central projection view and (d) geometry with labelling.

**Table 1**

Crystal data and structure refinement for  $3\beta$ -acetoxy cholest-5-ene.

Empirical formula	$C_{29}H_{48}O_2$
Formula mass	428.67
Wavelength ( $\lambda$ )	0.71073 Å
Crystal system	Monoclinic
Space group	$P2_1$
Unit cell dimensions	
$a$ , Å	16.585(2)
$b$ , Å	9.5175(12)
$c$ , Å	17.656(2)
$\alpha$ (deg)	90.000
$\beta$ (deg)	106.369(4)
$\gamma$ (deg)	90.000
Volume, Å <sup>3</sup>	2674.0(6)
No. of molecules per unit cell ( $Z$ )	4
Calculated density, Mg m <sup>-3</sup>	1.065
Absorption coefficient ( $\mu$ , mm <sup>-1</sup> )	0.064
$F(000)$	952
Crystal size	0.32 × 0.21 × 0.15 mm

$\theta$ range for data collection	2.38 to 25.50°
Limiting indices	-20<=h<=20, -11<=k<=11, -18<=l<=21
Reflections collected	19658
Data/restraints/parameters	9607/178/567
Goodness-of-fit on $F^2$	0.956
Final R indices [ $I > 2\sigma(I)$ ]	$R1 = 0.0686$ , $wR2 = 0.1363$
R indices (all data)	$R1 = 0.1757$ , $wR2 = 0.1786$

---

$R_1 = \Sigma ||F_o| - |F_c|| / \Sigma |F_o|$  with  $F_o^2 > 2\sigma(F_o^2)$ .  $wR_2 = [\Sigma w(|F_o^2| - |F_c^2|)^2 / \Sigma |F_o^2|]^2$

### 3.2. Molecular Hirshfeld surfaces

Hirshfeld surface is a valuable tool for understanding the surface characteristics of the molecules. It shows the area where molecules come into contact and therefore its analysis provides the additional insight into the intermolecular interactions within the crystal. The Hirshfeld surface is described by regions where the part of the electron density from the molecule of interest is equal to the contribution from the other molecules. The two distances are defined for each point on the surface:  $d_e$  (the distance from the point to the nearest nucleus external to the surface), and  $d_i$  (the distance to the nearest nucleus internal to the surface). The molecular Hirshfeld surfaces of 3 $\beta$ -acetoxy cholest-5-ene were generated using a standard (high) surface resolution with the 3D  $d_{norm}$  surfaces. The surfaces were mapped over a fixed color scale of -0.23 (red) to 1.2 Å (blue). The shape index and curvedness were mapped in the color range of -0.99 to 1 and of -4.0 to 0.4 respectively. The molecular Hirshfeld surface ( $d_{norm}$ , shape index and curvedness) of 3 $\beta$ -acetoxy cholest-5-ene are presented in Fig. 2. The normalized contact distances,  $d_{norm}$  were mapped into the Hirshfeld surfaces for comparison of intermolecular interactions in crystal structures. Negative values of  $d_{norm}$  as shown by the red color indicate contacts shorter than the sum of van der Waals radii. The white color visualizes intermolecular distances close to van der Waals contacts with  $d_{norm}$  equal to zero. In turn, positive  $d_{norm}$  values indicated by blue color define contacts longer than the sum of van der Waals radii. The bright red regions in the Hirshfeld

surface are appeared due to the O---H and C---H interaction in the compound. The H---H and C---C contacts can be seen by other visible spots on the surface correspond. Shape index describe the surface shape, and it is sensitive to very fine changes in surface shape, mainly in areas where the total curvature (or the curvedness) is very low. The information expressed by shape index is given with the 2D fingerprint plot. The flat areas of the surface have correspondence to low values of curvedness, while sharp curvature areas are related to high values of curvedness. This usually tends to divide the surface into patches, representing interactions between neighboring molecules. The 2D fingerprint plots can be decomposed to highlight close contacts of particular atom pair [11]. The 2D fingerprint plots, analyses all the intermolecular contacts simultaneously, revealed that the main intermolecular interactions in the present compound were C---H, H---H, O---H and C---C intermolecular interactions (Fig. 3). H---H interactions, which cover most of regions in the 2D fingerprint plots, have a major contribution to the total Hirshfeld surfaces (85.9%). The O---H contacts are appeared as distinct spikes pointing in the direction of the lower left of the plot. In these complementary regions one molecule acts as donor ( $d_e > d_i$ ) and the other as an acceptor ( $d_e < d_i$ ). The minimum value of ( $d_e + d_i$ ) i.e. the shortest contact is around 1.9Å which point out the significance of these interactions. The proportion of H---O interactions comprising 8.2% of the total Hirshfeld surfaces for the molecule. The top left and bottom right regions of the fingerprint plot are the characteristic “wings” which are identified as a result of C---H interactions. The decomposition of the fingerprint plot for H---C contacts comprised 5.4% of the total Hirshfeld surface area. Finally, C---C contacts comprised 0.5% of the total Hirshfeld surface area. Thus the nature of the interaction for the title compound is straightforwardly understood using Hirshfeld surface, with the results further highlighting the importance of the technique in mapping out the interactions within the crystal and this tool has very important

promise in crystal engineering. The Hirshfeld surface allows a much more detailed scrutiny by exhibiting all the intermolecular interactions and also by quantifying them in two dimensional fingerprint plot within the crystal.

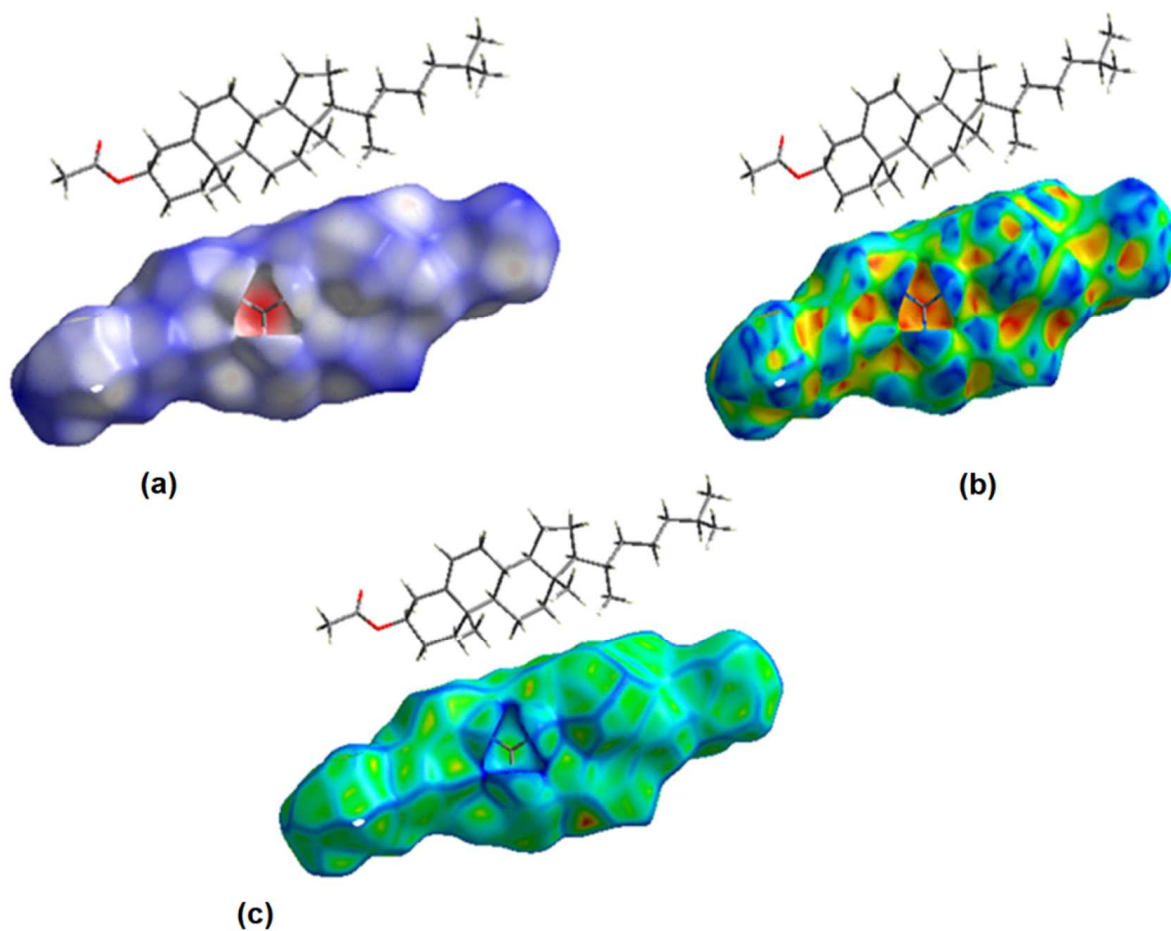


**Fig. 2.** Hirshfeld surfaces mapped with (a)  $d_{norm}$ , (b) surface index and (c) curvedness of 3β-acetoxy cholest-5-ene. The surfaces are shown as transparent to allow visualization of the orientation and conformation of the functional groups in the molecule.

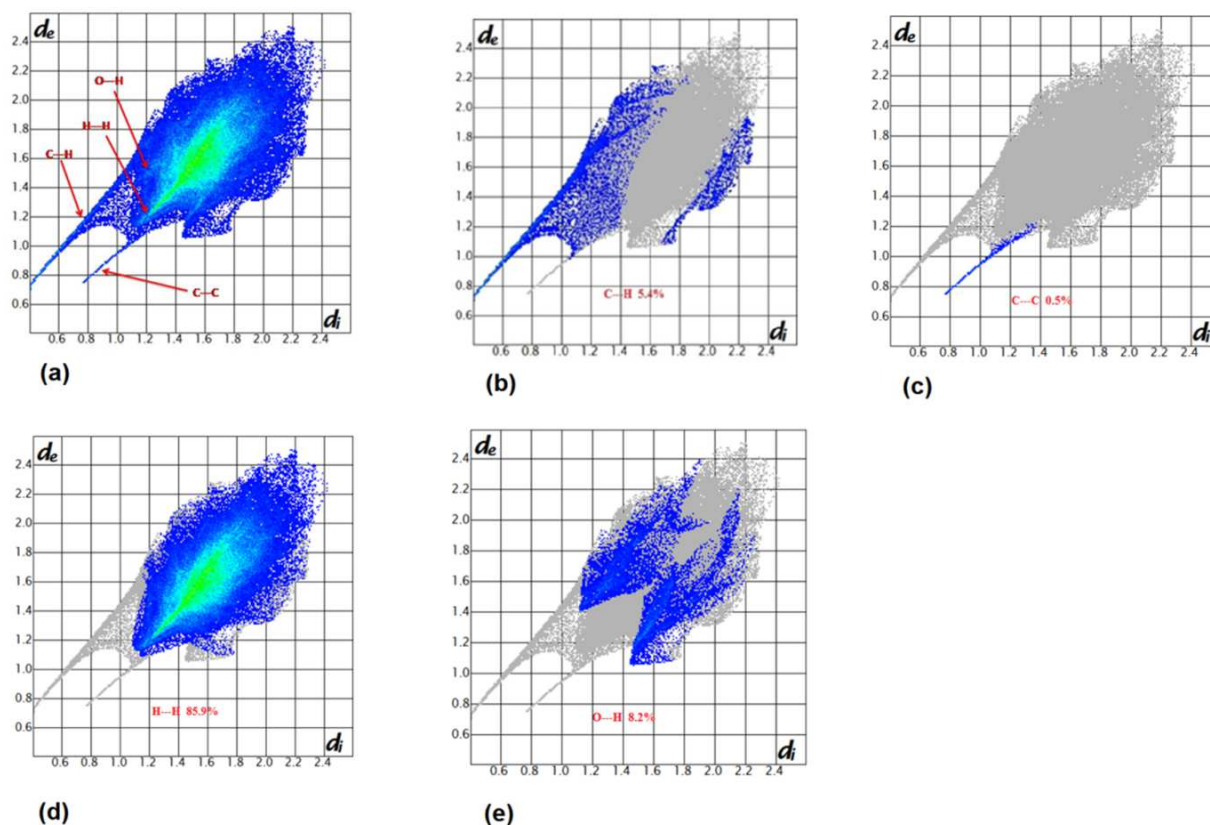


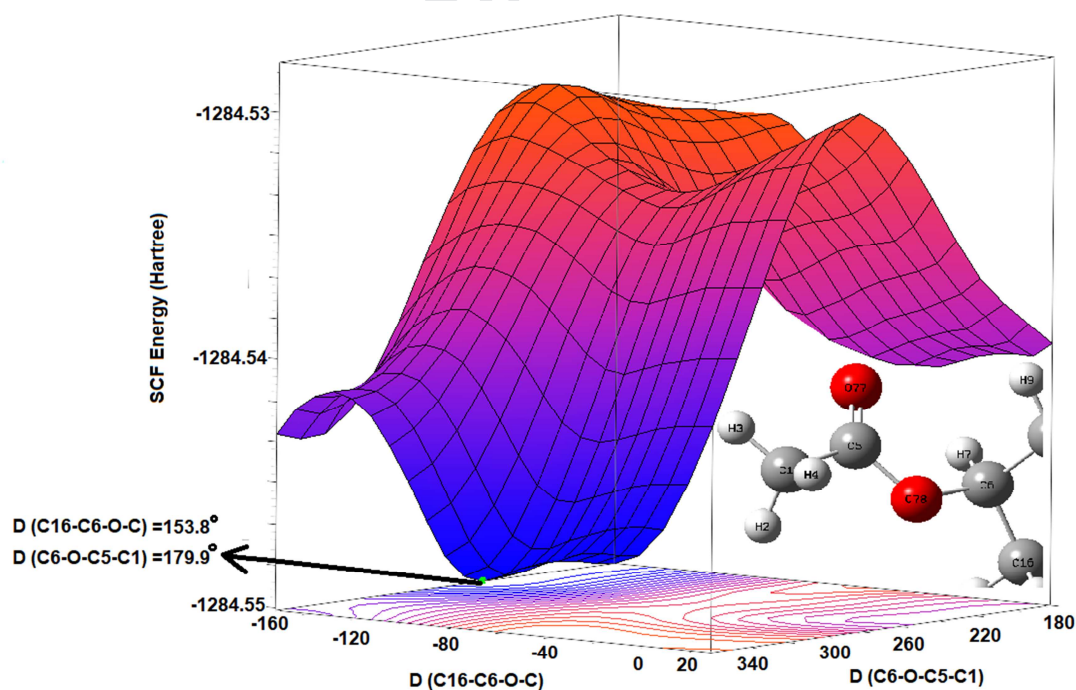
**Fig. 3.** 2D fingerprint plots of  $3\beta$ -acetoxy cholest-5-ene. (a) full (b) resolved into C-H (c) C-C (d) H-H (e) O-H contacts showing the percentages of contacts contributed to the total Hirshfeld surface area molecule.

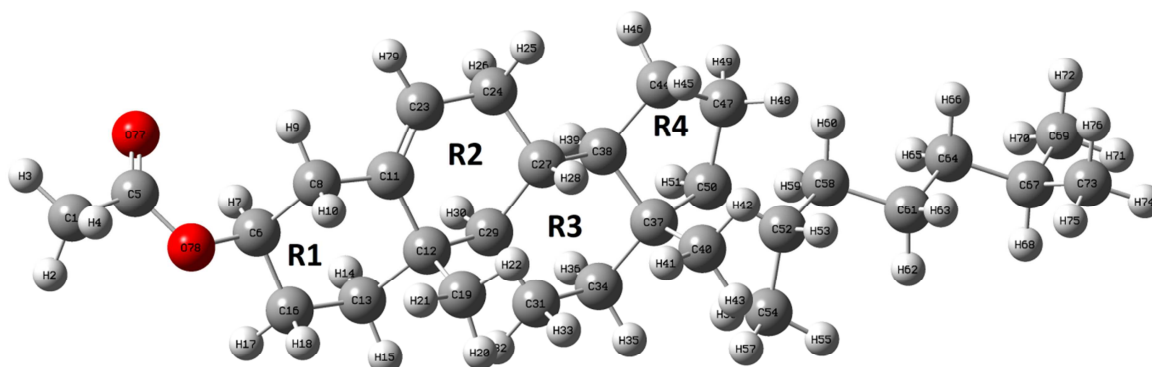
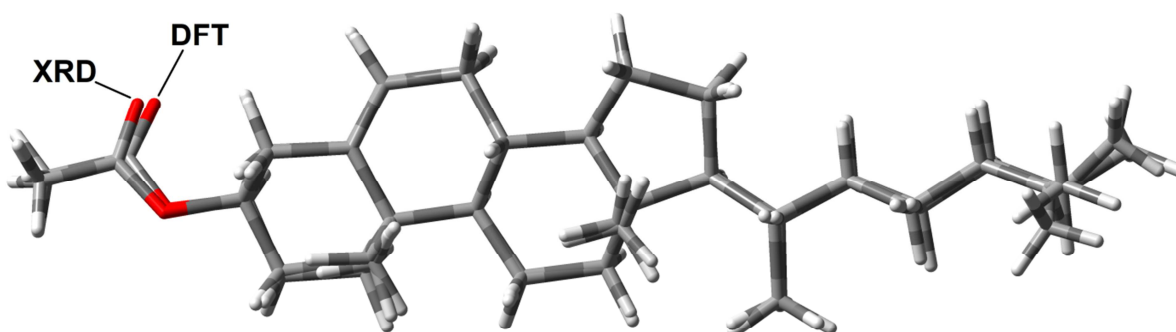
### 3.3. DFT calculation results

#### 3.3.1. Conformational search and molecular geometry

Potential energy surface (PES) scan has been performed to obtain the most stable structure by rotating acetoxy group of the present compound, Fig. 4. The dihedral angles i.e. C-C6-O-C5 and C6-O-C5-C1 for the most stable geometry on PES are found to be  $153.8^\circ$  (Exp.  $156.1^\circ$ ) and  $179.9^\circ$  (Exp.  $177.9^\circ$ ) respectively. The molecular geometry with  $\beta$ -acetoxy, obtained by PES

scan, is in good agreement with the XRD geometry. The optimized molecular structure (most stable geometry) of  $3\beta$ -acetoxy cholest-5-ene molecule along with numbering of atoms is shown in Fig. 5. The numbering scheme is used as per Fig. 5 to discuss DFT results. The minimum self-consistent field (SCF) energy and dipole moment are found to be -806233.7902 kcal/mol and 2.016 Debye, respectively. The comparison of some selected optimized geometrical parameters with the X-ray diffraction data is shown in Table 2. They are in a reasonable agreement as low values of RMSE and MAD ( $1-3^\circ$  for angles) are found. However, any discrepancies noted may be due to fact that the XRD data belongs to molecule with many surrounding interactions while the DFT results were obtained for molecule in isolated form. The molecular geometries obtained from DFT calculation and XRD experiment have been globally compared by superimposing atom by atom (Fig. 6) and RMSE value is found to be  $0.477 \text{ \AA}$  at B3LYP/6-311G(d,p) level of theory.



**Fig. 4.** PES scan of acetoxy group of  $3\beta$ -Acetoxy cholest-5-ene molecular geometry.**Fig. 5.** Optimized molecular geometry of  $3\beta$ -acetoxy cholest-5-ene.**Fig. 6.** Superimposed molecular structure of  $3\beta$ -acetoxy cholest-5-ene obtained by XRD and DFT.**Table 2**Some selected structural parameters of  $3\beta$ -acetoxy cholest-5-ene.

Bond lengths (Å)	<sup>a</sup> Exp.	B3LYP/6-311G(d,p)	Bond angles (°)	<sup>a</sup> Exp.	B3LYP/6-311G(d,p)
C1-C5	1.462	1.510	C1-C5-O	113.6	110.6
C5=O	1.214	1.205	C1-C5=O	124.9	125.2

C5-O	1.322	1.352	O=C5-O	121.4	124.2
O-C6	1.464	1.455	C5-O-C6	119.1	117.5
C6-C8	1.510	1.530	O-C6-C16	107.4	107.1
C6-C16	1.491	1.520	O-C6-C8	108.8	110.2
C11-C12	1.514	1.533	C8-C6-C16	112.25	111.1
C11=C23	1.312	1.335	C47-C50-C52	112.3	112.5
C8-C11	1.506	1.516	C37-C50-C52	119.3	119.7
C50-C52	1.539	1.544	C69-C67-C73	114.2	110.5
MAD		0.020			1.5
RMSE		0.024			1.9
Dihedral angles (°)			Dihedral angles (°)		
C1-C5-O78-C6	177.9	179.9	O77=C5-O78-C6	0.5	0.2
C16-C6-C8-C11	50.3	53.9	O78-C6-C8-C11	169.0	172.5
O78-C6-C16-C13	172.0	176.6	C8-C6-O78-C5	82.2	85.2
C16-C6-O78-C5	156.1	153.8	C37-C50-C52-C54	58.7	55.6
C37-C50-C52-C58	177.0	179.6	C47-C50-C52-C54	179.6	177.2
<b>MAD</b>					2.7
<b>RMSE</b>					2.9

<sup>a</sup> Obtained from single crystal XRD data; numbering scheme is adopted as per Fig. 5

RMSE: root mean square error, MAD: mean absolute deviation

### 3.3.2. Vibrational analysis

The present compound consists of 79 atoms consequently it has 231 normal vibrations. Out of these, some important vibrational modes have been discussed. Present compound consists of four rings (six member R1/R2/R3 and five member R4, Fig. 5) with CH/CH<sub>2</sub>/CH<sub>3</sub> groups, carbon chain with CH/CH<sub>2</sub>/CH<sub>3</sub> groups and one acetoxy group. Some important vibrational assignments and comparison of FTIR band frequencies and intensities with the theoretical one are presented in Table 3. Only the major contributions of the vibrations are mentioned in the Table 3. This table is self-explanatory for the vibrational assignments however some vibrations need discussions. The low values of deviations RMSE and MAD show the reasonable agreement between theoretical (scaled) and experimental IR frequencies. The observed FTIR and simulated IR spectra of the compound are shown in Fig. 7. In general, aliphatic CH<sub>3</sub> and acyclic CH<sub>2</sub> stretching vibrations occur in the regions 2975-2865 cm<sup>-1</sup> and 2940-2880 cm<sup>-1</sup> respectively [34]. The IR bands due to CH<sub>3</sub> symmetric bending (Umbrella) vibration appear often in the region

1420-1375  $\text{cm}^{-1}$  [34]. These vibrations are observed in the present FTIR band within the said region as shown in Table 3. Scaled IR frequencies of these vibrations are found close with the experimental one. The strong IR band observed at 1736  $\text{cm}^{-1}$  is assigned to C=O stretching vibration in acetoxy group of the compound. The scaled frequency of C=O stretching vibration is 1746  $\text{cm}^{-1}$  for the present molecule. The C-O stretching vibration is assigned to the strong band observed at 1246  $\text{cm}^{-1}$ . The calculated harmonic frequency of this vibration is 1257  $\text{cm}^{-1}$ . These vibrations of acetoxy group are found in agreement with those obtained theoretically as well as of reported data in literature [35]. Vibrational modes found below 1000  $\text{cm}^{-1}$  are mixed with skeleton vibrations.

**Table 3**

Important vibrational frequencies ( $\text{cm}^{-1}$ ), integrated intensity ( $\text{km/mol}$ ) and assignments.

FTIR	harmonic	scaled <sup>a</sup>	IR intensity	Assignment <sup>b</sup>
2948vs	3078	2976	82.7	$\nu$ CH <sub>3</sub> (C-chain)
2936vs	3071	2969	86.9	$\nu$ C-H (R1, R3)
2906sh	3016	2917	56.6	$\nu$ CH <sub>2</sub> (C-chain)
2870sh	2972	2874	28.9	$\nu$ C-H (R2)
1736vs	1805	1746	209.7	$\nu$ C5=O
1670w	1726	1669	2.7	$\nu$ C=C (R2)
1465s	1515	1465	14.9	$\beta$ C-H
1442sh	1494	1444	4.4	$\beta$ C-H (R3,R4,C-chain)
1368s	1416	1369	10.3	$\beta$ CH <sub>3</sub> (umbrella) + $\beta$ C-H
1312w	1358	1313	1.3	$\beta$ C-H
1246vs	1257	1216	491.2	$\nu$ C5-O + $\beta$ C-H
1137m	1177	1138	7.6	$\beta_{\text{twist}}$ CH <sub>2</sub> + $\beta$ C-C-C + $\gamma$ CH <sub>3</sub>
1085w	1123	1086	2.2	$\beta$ C-H + $\nu$ C-C + $\beta$ C-C-C
1032s	1047	1013	173.8	[ $\gamma$ CH <sub>3</sub> + $\nu$ C6-O] (acetoxy group)
980sh	1038	1004	40.6	$\gamma$ CH <sub>3</sub> (acetoxy group) + $\nu$ C-C + $\beta$ C-C-C
956m	988	956	3.6	$\gamma$ CH <sub>3</sub> (acetoxy group, R2) + $\nu$ C6-O + $\nu$ C-C
902m	937	906	4.9	$\beta$ C-C-C + $\gamma$ [CH <sub>2</sub> + CH <sub>3</sub> ] (rings, C-chain)
800m	854	826	4.3	$\gamma$ C23-H + $\beta_{\text{rock}}$ CH <sub>2</sub> (rings)
738m	747	722	2.7	[ $\nu$ C-C + $\beta$ C-C-C] (rings) + $\beta_{\text{rock}}$ CH <sub>2</sub> (R4)
612m	625	604	7.0	$\beta$ C-C-C (rings) + $\gamma$ C-H
<b>RMSE</b>	66	16		
<b>MAD</b>	55	11		

Abbreviation used: vs-very strong, s-strong, m-medium intensity, sh-shoulder, w-weak, v-

stretching,  $\beta$ - bending motion,  $\gamma$  -out-plane deformation vibrations, RMSE: root mean square error (in  $\text{cm}^{-1}$ ), MAD: mean absolute deviation (in  $\text{cm}^{-1}$ )

<sup>a</sup> harmonic wavenumbers were scaled by factor 0.967 [30].

<sup>b</sup> vibrations having major contribution; numbering scheme is adopted as per Fig. 5

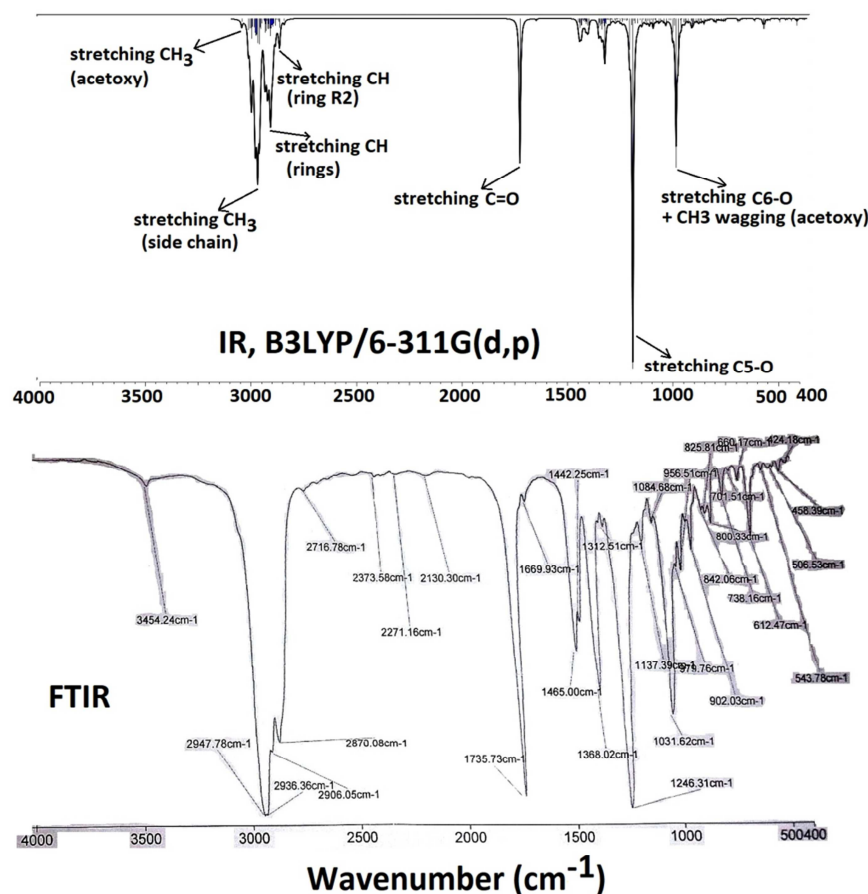


**Fig. 7.** Simulated and experiment IR spectra 3β-acetoxy cholest-5-ene.

### 3.3.3. NMR spectra

The <sup>1</sup>H NMR, <sup>13</sup>C NMR and Distortionless Enhancement by Polarization Transfer (DEPT) studies confirmed the molecular structure of 3β-acetoxy cholest-5-ene. The recorded <sup>1</sup>H and <sup>13</sup>C-NMR spectra of the molecule in CDCl<sub>3</sub> are compared with the theoretical one obtained at GIAO-B3LYP/6-311G(d,p)/IEF-PCM. They are found in good agreement. Experimental and simulated

NMR spectra ( $^1\text{H}$ ,  $^{13}\text{C}$ ) are presented in Fig. S1- S4 (supplementary files). The numbering of atoms was used as per Fig. 5. Most of the proton NMR signals are observed within the narrow region 0-3 ppm may be due to relatively high electron density over the nuclei (shielding effect). Two  $^1\text{H}$ -NMR signals observed in the region 4-6 ppm are assigned to olefinic proton at  $\delta$  5.4 and 4.5  $\delta$  for C3 $\alpha$ -proton. The corresponding theoretical chemical shift values are found to be 5.7 ppm and 4.5 ppm respectively for olefinic proton (H79) and C3 $\alpha$ -proton (H7). These are identified relatively at high ppm value because of low electron density over these nuclei. In the  $^{13}\text{C}$ -NMR spectrum, the signals are appeared in the region 0-180 ppm. Most of the signals are occurred in the region 0-80 ppm while three signals are appeared at high ppm values (120-180). These signals observed within range 120-180 ppm are due to C=O of acetoxy group and C=C. These carbon atoms have shown their presence at high ppm because these found with respectively large positive and almost zero charges (Fig. S5). It is often extra difficult to obtain a full aspect from a simple  $^{13}\text{C}$  spectrum, particularly if there is overlap in the spectral like our case. An alternative approach would be to acquire a DEPT spectrum (Fig. S6). The DEPT sequence produces signals only for protonated carbons by changing the flip angle of the final  $^1\text{H}$  pulse ( $45^\circ$ ,  $90^\circ$ , or  $135^\circ$ ). The DEPT with flip angle  $45^\circ$  detects signals for CH,  $\text{CH}_2$  and  $\text{CH}_3$ , with the same sign. The DEPT- $90^\circ$  provides only CH peaks. The DEPT- $135^\circ$  gives signals with positive sign for CH and  $\text{CH}_3$  while negative peaks for  $\text{CH}_2$ . In the DEPT- $135^\circ$  the  $^{13}\text{C}$  signal enhancement is achieved by polarization transfer from  $^1\text{H}$  to  $^{13}\text{C}$ . Other advantage of DEPT spectra over simple carbon NMR spectra is its ability to identify protonated carbon peaks that overlap one of the deuterated solvent peaks [36]. The nature of each carbon in the compound was deduced through DEPT spectrum (Fig. S6) by polarization pulses of  $135^\circ$ , obtaining negative signals (down) for  $\text{CH}_2$  groups while positive signals (up) for CH,  $\text{CH}_3$ . The DEPT- $135^\circ$  showed

the existence of six  $sp^3$  methyl, eleven  $sp^3$  methylene and eight methine (seven  $sp^3$  and one  $sp^2$ ) carbons.

#### 3.3.4. Other molecular properties

Quantum mechanical parameters describing various molecular properties obtained at B3LYP/6-311G(d,p) level are tabulated in Table 4. The donor-acceptor NBO hyperconjugative interaction energies,  $E^{(2)}$ , were estimated at same level of theory to investigate charge delocalization within the molecule. The strong hyperconjugative interactions for the present compound are predicted for LP (2) O78  $\rightarrow$   $\pi^*(C5=O77)$ , LP (2) O77  $\rightarrow$   $\sigma^*(C1 - C5)$  and LP (2) O77  $\rightarrow$   $\sigma^*(C5 - O78)$  with  $E^{(2)}$  values 47, 18 and 32 kcal/mol respectively. The hybridization of the atoms and the electron density (ED, in %) of atom in localized electron pair bond for acetoxy group of present compound is presented in Table 5. A bonding orbital for  $\sigma$  C5=O77 with occupancy 1.99652 has 34.09% C5 character in a  $sp^{1.91}$  hybrid and 65.91% O77 character in a  $sp^{1.35}$  hybrid while for  $\pi$  C5=O77 with occupancy 1.99031 has 30.40% C5 character in a  $sp^{1.00}$  hybrid and 69.60% O77 character in a  $sp^{99.99}$  hybrid. The  $sp^{1.91}$  hybrid on carbon and  $sp^{1.35}$  hybrid on oxygen atom have respectively 65.50% and 57.38%  $p$ -character for  $\sigma$  C5=O77, while for  $\pi$  C5=O77 the  $sp^{1.00}$  hybrid on carbon and  $sp^{99.99}$  hybrid on oxygen atom have respectively 99.48% and 99.87%  $p$ -character. In Table 5, oxygen (O78) has larger polarization coefficient (0.8359) because of higher electronegativity. Natural atomic charges obtained by NBO analysis are shown in Fig. S5. The mean first hyperpolarizability of present compound is found to be  $0.6481 \times 10^{-30}$  esu, which is about 2 times greater than of urea ( $0.3728 \times 10^{-30}$  esu) [37]. This value shows that the  $3\beta$ -acetoxy cholest-5-ene may be used for NLO application. The MEP plot is obtained by mapping electrostatic potential onto total electron density of the molecule to know its binding sites i.e. nucleophilic/electrophilic (Fig. 8). The electrostatic potentials are shown over the surface in

terms of colour scheme. The regions with blue, green and red/ yellow colours define the positive, zero and negative values of the potential respectively. In the MEP plot, most of the regions over the molecule shown by green colour are characterized as neutral part of the molecule. The regions over the O77 and O7 atoms (acetoxy group) represent the negative potential (dark red/yellow coloured/ high electron density). The light blue colour regions spotted over the H-atoms of molecule are characterized by positive potential. The frontier molecular orbitals i.e. HOMO and LUMO play important role in chemical reactions. The HOMO, LUMO energy Eigen values and HOMO-LUMO energy gap help to determine the chemical reactivity of molecules. The spatial plot of HOMO and LUMO of the present molecule is shown in Fig. 9. The HOMO and LUMO energy Eigen values, HOMO-LUMO energy gap and various global reactivity descriptors computed at B3LYP/6-311G(d,p) level of theory are presented in Table 4. In Fig. 9, the HOMO is delocalized mainly over the ring (R1 and R2), while the LUMO is delocalized mainly over the acetoxy group. Thus, HOMO-LUMO plot shows that these frontier molecular orbitals are localized over some part of the molecule. HOMO and LUMO are found completely absent over the other rings and side carbon chain. Therefore, these regions may not participate much in chemical reactions as its molecular orbitals are of too large in energy for the reactions. A large value of HOMO-LUMO gap (~6 eV) exhibits good thermodynamic stability and low chemical reactivity. The global reactivity descriptors based on HOMO and LUMO energy Eigen values are presented in Table 4. These chemical descriptors were estimated using relations given in literatures [38-44]. These global descriptors are important parameters for molecule in quantitative structure – activity relationship (QSAR) modeling [45].

**Table 4**

Some quantum chemical parameters for 3 $\beta$ -acetoxy cholest-5-ene.

Parameters	B3LYP/6-311G(d,p)	Parameters	B3LYP/6-311G(d,p)
Minimum SCF energy (kcal/mol)	-806233.7902	E <sub>HOMO</sub> (eV)	-6.460
Dipole Moment (Debye)	2.0159	E <sub>LUMO</sub> (eV)	0.270
Polarizability ( $\alpha$ ) in a.u.	328.7104	HOMO-LUMO Gap (eV)	6.190
HyperPolarizability ( $\beta$ ) in e.s.u	0.6481 x 10 <sup>-30</sup>	Global reactivity descriptors (eV)	
Zero point vibrational energy (kcal/mol)	451.6656	Hardness	3.365
Total thermal energy (kcal/mol)	472.435	Chemical potential	-3.095
Heat Capacity (Cv) cal/mol-kelvin	130.317	Electron affinity	-0.270
Entropy (S) cal/mol-kelvin	209.564	Electrophilicity	1.423
		Electronegativity	3.095
		Ionization potential	6.460
		Softness (eV <sup>-1</sup> )	0.148
		Electrofugality	6.201
		Nucleofugality	0.011

**Table 5**

NBO analysis of acetoxy group in 3 $\beta$ -acetoxy cholest-5-ene at B3LYP/6-311G(d,p) level of theory

Bond (A-B) <sup>a</sup>	Occupancy	ED <sub>A</sub> %	ED <sub>B</sub> %	NBO (% p character)
$\sigma$ C1 - H2	1.97660	60.79	39.21	0.7797sp <sup>3.22</sup> (76.26) <sub>C</sub> + 0.6262sp <sup>0.00</sup> (0.04) <sub>H</sub>
$\sigma$ C1 - H3	1.98734	60.80	39.20	0.7797sp <sup>3.10</sup> (75.55) <sub>C</sub> + 0.6261sp <sup>0.00</sup> (0.04) <sub>H</sub>
$\sigma$ C1 - H4	1.97389	60.78	39.22	0.7797sp <sup>3.26</sup> (76.49) <sub>C</sub> + 0.6262sp <sup>0.00</sup> (0.04) <sub>H</sub>
$\sigma$ C1 - C5	1.98119	51.55	48.45	0.7180 sp <sup>2.50</sup> (71.41) <sub>C</sub> + 0.6961 sp <sup>1.66</sup> (62.32) <sub>C</sub>
$\sigma$ C5 - O77	1.99652	34.09	65.91	0.5838 sp <sup>1.91</sup> (65.50) <sub>C</sub> + 0.8119 sp <sup>1.35</sup> (57.38) <sub>O</sub>
$\pi$ C5 - O77	1.99031	30.40	69.60	0.5514 sp <sup>1.00</sup> (99.48) <sub>C</sub> + 0.8342 sp <sup>99.99</sup> (99.87) <sub>O</sub>
$\sigma$ C5 - O78	1.99197	30.78	69.22	0.5548 sp <sup>2.57</sup> (71.82) <sub>C</sub> + 0.8320 sp <sup>2.11</sup> (67.84) <sub>O</sub>
$\sigma$ C6 - O78	1.98513	30.13	69.87	0.5489 sp <sup>4.48</sup> (81.53) <sub>C</sub> + 0.8359 sp <sup>2.29</sup> (69.54) <sub>O</sub>
LP (1) O77	1.97657			sp <sup>0.74</sup> (42.51)
LP (2) O77	1.84856			sp <sup>1.00</sup> (99.92)
LP (1) O78	1.96488			sp <sup>1.67</sup> (62.48)
LP (2) O78	1.79556			sp <sup>1.00</sup> (99.95)

Abbreviation used: ED: electron density

<sup>a</sup> numbering scheme is adopted as per Fig. 5

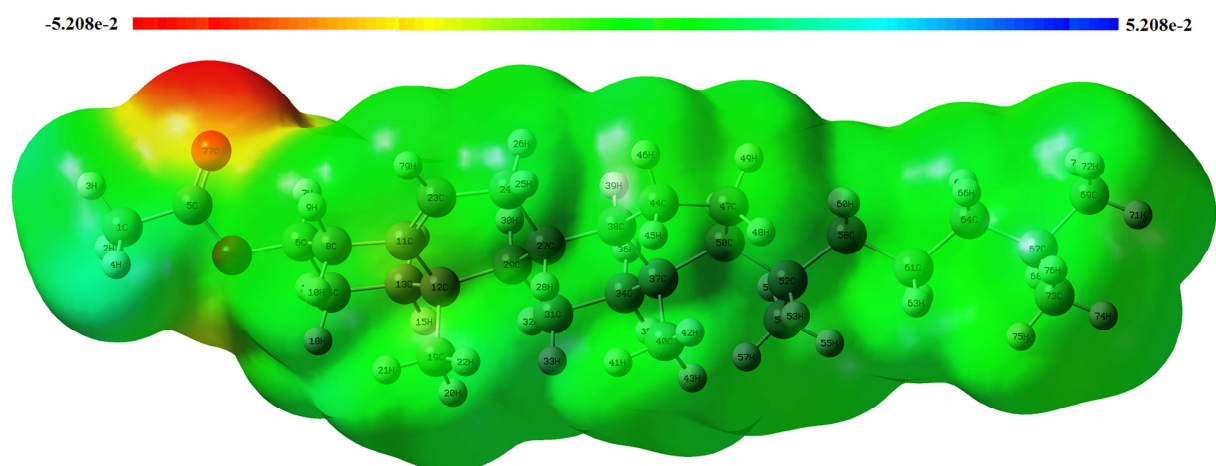


Fig. 8. MEP plot of 3β-acetoxycholest-5-ene.

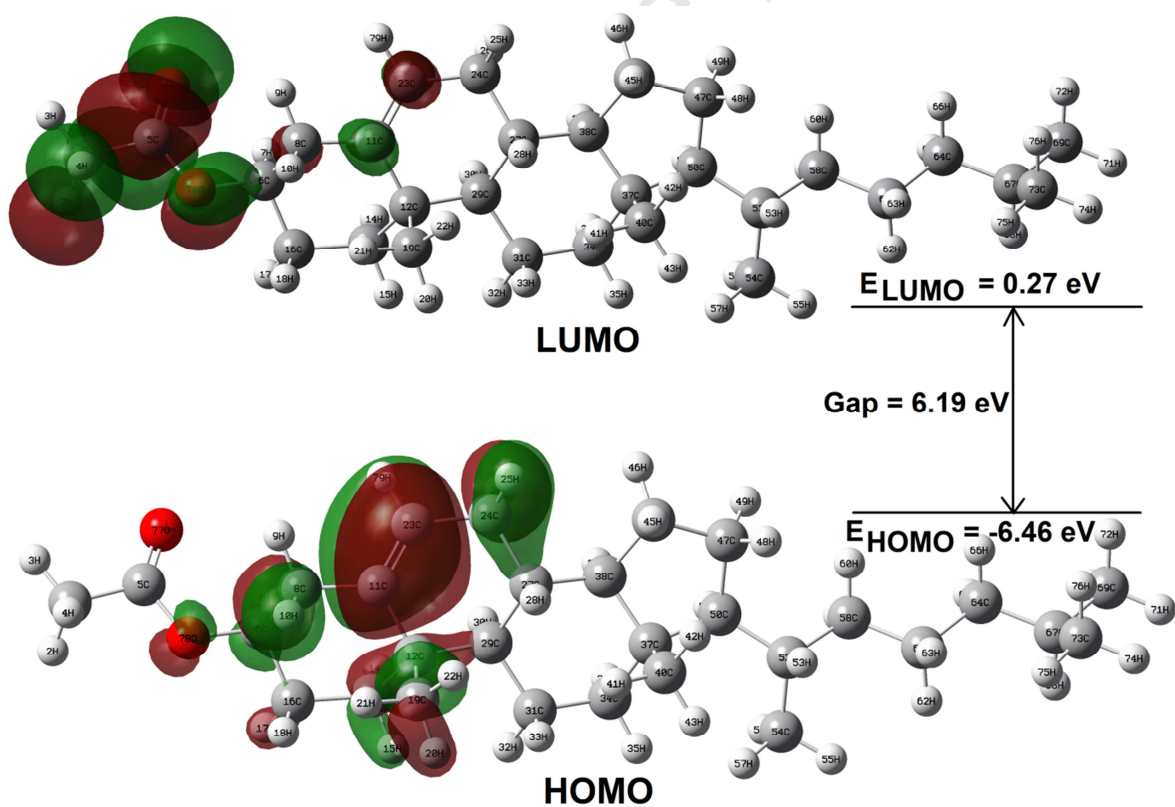


Fig. 9. HOMO and LUMO spatial plots.

### 3.4. Elemental analysis

To determining the constituents and purity compositions of the crystallized compound, analysis of carbon and hydrogen was carried out. The calculated elemental analysis of  $C_{29}H_{48}O_2$  is C, 81.25 and H, 11.29 (%) and the experimental; C, 81.29; H, 11.26 (%). As we can see the experimental and calculated values within  $\pm 0.4\%$ , confirming the purity of compound  $>95\%$ .

### 3.5. Conformations of the compound in solution and solid state

We examined the conformations of crystallized compound in solution *via* NMR and solid state through X-ray. The angles were measured from CIF files (solid state data). Nuclear Overhauser Effect Spectroscopy (NOESY) spectrum of  $3\beta$ -Acetoxy cholest-5-ene has been also reported. This spectrum exhibits signature due to interactions within the molecule through space and also shows the correlation between protons which are close enough in space. In spectrum, the cross peaks signals are appeared due to protons that are close in space. The coupling constants ( $^3J_{H-H}$ ) were obtained by analysis of NOESY NMR (Fig. S7) of the molecule in  $CDCl_3$ , and angles were determined using the on-line interactive data table. When this  $^3J_{H-H}$  corresponded to two or more possible angles, the nearby one (between  $-90$  and  $+90^\circ$  from the solid state angle) was chosen [46]. The estimate of the dihedral angles deduced from the measured coupling constants are presented in Table 6. Remarkably, we analyzed less difference in the conformations of the compound in the solid state and in solution phase, showing that the bending of rings at the A, B junction was also less in solution phase than in the solid phase.

**Table 6**

Comparison of torsion angles of  $3\beta$ -acetoxy cholest-5-ene.

Torsion angle <sup>a</sup>	Measured angle	$^3J_{H-H}$ (Hz)	Calculated
----------------------------	----------------	------------------	------------

	(solid state)		(solution)
C10-C5-C4-C3	127.27		
C4-C5-C10-C11	176.90		
C8-C7-C6-C13	174.93		
C7-C6-C13-C12	156.70		
H10-C10-C11-H11 $\beta$	43.59	2.75	53.34
H10-C10-C11-H11 $\alpha$	-74.14		
H11 $\alpha$ -C11-C12-H12	167.16	8.7	166.46
H11 $\beta$ - C11-C12-H12	49.37	4.4	42.09

<sup>a</sup> Fig. 1(d)

### 3.6. Scanning electron microscopy

The surface morphology of the crystal was studied through scanning electron microscopy (SEM). The SEM micrograph (Fig. 10) indicated presence of brick-shaped, some irregular shaped particles and it shows that the crystals grown in big size.

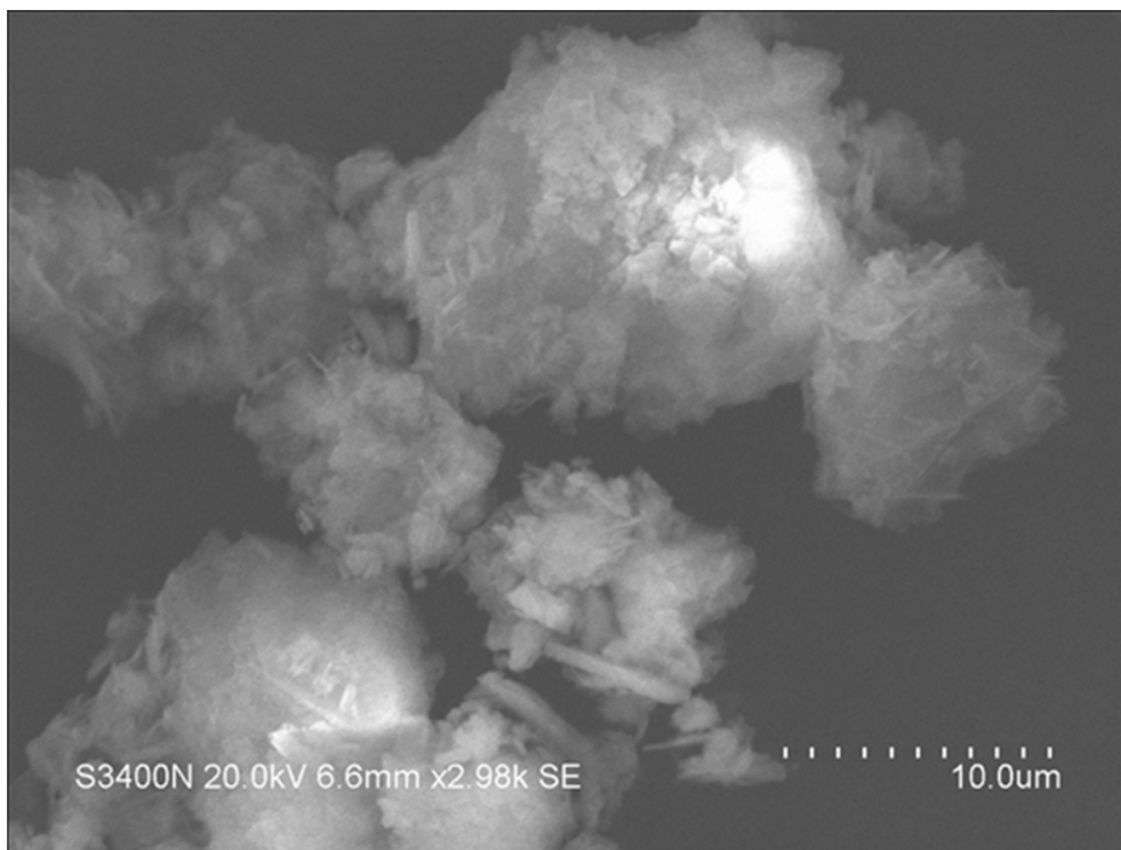


Fig. 10. SEM micrograph of  $3\beta$ -acetoxy cholest-5-ene.

### 3.7. Density measurement

The calculated density of  $C_{29}H_{48}O_2$  was determined by taking the ratio of the cell mass to cell volume. The equation for the density is defined as  $\rho_{\text{calc}} = MZ/NV$ , where  $M$  is the chemical formula weight of crystals,  $Z$  is the number of formula units in one cell,  $N$  is Avogadro's number and  $V$  is the volume of the unit cell. According to the crystallographic data, it is observed that  $a = 16.585(2) \text{ \AA}$ ,  $b = 9.5175(12)$ ,  $c = 17.656(2)$ ,  $M = 428.67$ ,  $Z = 4$ , and  $V = 2674.0(6) \text{ \AA}^3$ . So the calculated density of the crystal was found to be  $1.065 \text{ Mg m}^{-3}$ . Experimentally, the density of the  $3\beta$ -acetoxy cholest-5-ene crystal was measured using the buoyancy method at temperature 22

°C in silicon oil. This experimental density of the as-grown crystal is found to be  $1.069 \pm 0.003$  Mg m<sup>-3</sup>, which is almost equal to the calculated density.

### 3.8. Deliquescence test

To verify the deliquescence of the 3 $\beta$ -acetoxy cholest-5-ene crystal, at the room temperature the crystal sample was subjected to air atmosphere without any protection [47]. At the starting, it was transparent, and the weight was about 0.7872 g. After five days, we could not observe any change in the weight (0.7875 g). Still, after 15 days we could not notice changes in the weight (0.7880 g). These observations undoubtedly indicate that 3 $\beta$ -acetoxy cholest-5-ene has good deliquescence resistance and is stable in air.

### 3.9. Thermogravimetric analysis (TGA)

TGA was performed to know the purity and thermal stability of the present crystal. The TG curve of crystal revealed that it is stable up to 280 °C and does not undergo any phase transition Fig. S8. The disintegration process started after 280 °C and continued till complete decomposition and at 450 °C, all the mass was lost and nothing was left as residue. Thus, no weight loss or phase transition around or before its melting point was observed which confirmed the nonexistence of any lattice entrapped solvent or moisture on the grown material.

### 3.8. Powder XRD

The powder XRD pattern of 3 $\beta$ -acetoxy cholest-5-ene is shown in Fig. S9. The XRD profiles showed that grown crystal was of single phase without detectable impurity. The appearances of sharp and strong peaks confirmed the good crystallinity of the grown crystals. The lattice

parameters of crystals were calculated theoretically using the powder XRD data and were found in good agreement with the values obtained from single crystals.

#### 4. Conclusion

In the present work, we have demonstrated synthesis of  $3\beta$ -acetoxy cholest-5-ene from cholesterol using  $\text{Zn}(\text{OTf})_2$ . The crystal structure was solved by using single crystal X-ray diffraction data. In addition spectral, thermal and morphological properties have also been investigated. Hirshfeld surface and fingerprint plot analysis of the title compound provided insight into the intermolecular interactions, which are crucial in crystal packing. TGA has confirmed the nonexistence of any lattice entrapped solvent or moisture on the grown material. Potential energy surface (PES) scan of the present compound has confirmed the molecular geometry with  $\beta$ -acetoxy which is found in agreement with its XRD geometry. The low values of deviations RMSE and MAD have shown reasonable agreement between theoretical and experimental IR frequencies. The mean first hyperpolarizability value of present compound is found to about 2 times greater than of urea, therefore, the  $3\beta$ -acetoxy cholest-5-ene may be a NLO material. The present experimental data on molecular geometry, FTIR and NMR spectra has successfully validated the B3LYP/6-311G(d,p) calculations.

#### Acknowledgments

The authors would like to thank the Chairman, Department of Chemistry, Aligarh Muslim University, Aligarh for providing necessary research facilities. AM acknowledges UGC, New Delhi, India for providing JSR fellowship during his Ph.D.

## Reference

- [1] I. Tabas, Consequences of cellular cholesterol accumulation: basic concepts and physiological implications, *J. Clin. Invest.* 110 (2002) 905-911, <https://doi.org/10.1172/JCI16452>
- [2] L.E. Gerweck, S. Vijayappa, S. Kozin, Tumor pH controls the in vivo efficacy of weak acid and base chemotherapeutics, *Mol. Cancer. Ther.* 5 (2006) 1275-1279, <https://doi.org/10.1158/1535-7163.MCT-06-0024>
- [3] M. Viji, R. Nagarajan,  $\text{RuCl}_3/\text{SnCl}_2$  mediated synthesis of pyrrolo[2,3-c]carbazoles and consequent preparation of indolo[2,3-c]carbazoles, *Tetrahedron* 68 (2012) 2453-2458, <https://doi.org/10.1016/j.tet.2012.01.070>
- [4] K. Warabi, S. Matsunaga, R.W. van Soest, N. Fusetani, Dictyodendrins A-E, the first telomerase-inhibitory marine natural products from the sponge dictyodendrilla verongiformis, *J. Org. Chem.* 68 (2003) 2765-2770, <https://doi.org/10.1021/jo0267910>
- [5] S. Madhankumar, P. Muthuraja, M. Dhandapani, Structural characterization, quantum chemical calculations and hirshfeld surface analysis of a new third order harmonic organic crystal: 2-amino-4-methylpyridinium benzilate, *J. Mol. Struct.* 1201 (2020) 127151-127161, <https://doi.org/10.1016/j.molstruc.2019.127151>
- [6] J.J. McKinnon, D. Jayatilaka, M.A. Spackman, Towards quantitative analysis of intermolecular interactions with hirshfeld surfaces, *Chem. Commun.* (2007) 3814-3816, <https://doi.org/10.1039/B704980C>
- [7] H.F. Clausen, M.S. Chevallier, M.A. Spackman, B.B. Iversen, Three new co-crystals of hydroquinone: crystal structures and hirshfeld surface analysis of intermolecular interactions, *New J. Chem.* 34 (2010) 193-199, <https://doi.org/10.1039/B9NJ00463G>
- [8] S.K. Seth, I. Saha, C. Estarellas, A. Frontera, T. Kar, S. Mukhopadhyay, Supramolecular self-Assembly of M-IDA complexes involving lone-pair $\cdots\pi$  interactions: crystal structures, hirshfeld surface analysis, and DFT calculations

- [H<sub>2</sub>-IDA = iminodiacetic acid, M = Cu(II), Ni(II)], *Cryst. Growth Des.* 11 (2011) 3250-3265, <https://doi.org/10.1021/cg200506q>
- [9] A.L. Rohl, M. Moret, W. Kaminsky, K. Claborn, J.J. Mckinnon, B. Kahr, Hirshfeld surfaces identify inadequacies in computations of intermolecular interactions in crystals: pentamorphic 1,8-dihydroxyanthraquinone, *Cryst. Growth Des.* 8 (2008) 4517-4525, <https://doi.org/10.1021/cg8005212>
- [10] A. Parkin, G. Barr, W. Dong, C.J. Gilmore, D. Jayatilaka, J.J. Mckinnon, M.A. Spackman, C.C. Wilson, Comparing entire crystal structures: structural genetic fingerprinting, *CrystEngComm* 9 (2007) 648-652, <https://doi.org/10.1039/B704177B>
- [11] Shamsuzzaman, H. Khanam, A. Mashrai, M. Ahmad, Y.N. Mabkhot, W. Frey, N. Siddiqui, Synthesis, growth, spectral, thermal and crystallographic studies of 5 $\alpha$ ,6 $\alpha$ -epoxycholestane single crystals, *J. Cryst. Growth* 384 (2013) 135-143, <https://doi.org/10.1016/j.jcrysgro.2013.08.037>
- [12] Shamsuzzaman, A. Mashrai, H. Khanam, Y.N. Mabkhot, W. Frey, 3 $\beta$ -Acetoxy-6-nitrocholest-5-ene: crystal structure, thermal, optical and dielectrical behavior, *J. Mol. Struct.* 1063 (2014) 219-225, <https://doi.org/10.1016/j.molstruc.2014.01.031>
- [13] Shamsuzzaman, H. Khanam, A. Mashrai, M. Asif, A. Ali, A. Barakat, Y.N. Mabkhot, Synthesis, crystal structure, hirshfeld surfaces, and thermal, mechanical and dielectrical properties of cholest-5-ene, *J. Taibah Univ. Sci.* 11 (2017) 141-150, <https://doi.org/10.1016/j.jtusci.2016.01.001>
- [14] S. Uzzaman, H. Khanam, A. Mashrai, Y.N. Mabkhot, A. Husain, 6-Hydroxyimino-5 $\alpha$ -cholestane, *Acta Cryst.* E68 (2012) o3037-o3038, <https://doi.org/10.1107/S1600536812040093>
- [15] H. Khanam, A. Mashrai, N. Siddiqui, M. Ahmad, Shamsuzzaman, M.J. Alam, S. Ahmad, Structural elucidation, density functional calculations and contribution of intermolecular interactions in cholest-4-en-3-one crystals: Insights from X-ray and hirshfeld surface analysis, *J. Mol. Struct.* 1084 (2015) 274-283, <https://doi.org/10.1016/j.molstruc.2014.12.027>
- [16] M. Alam, M.J. Alam, S.A.A. Nami, D.-U. Lee, M. Azam, S. Ahmad, Computational and anti-tumor studies of 7a-Aza-B-homostigmast-5-eno [7a, 7-d] tetrazole-3 $\beta$ -yl

- chloride, J. Mol. Struct. 1108 (2016) 411-426, <https://doi.org/10.1016/j.molstruc.2015.12.030>
- [17] M. Alam, M.J. Alam, S.A.A. Nami, M.S. Khan, S. Ahmad, D.-U. Lee, DFT, hirshfeld surfaces, spectral and in vivo cytotoxic studies of 7a-Aza-B-homostigmast-5-eno [7a,7-d] tetrazole, J. Mol. Struct. 1099 (2015) 588-600, <https://doi.org/10.1016/j.molstruc.2015.07.017>
- [18] M.J. Alam, A.U. Khan, M. Alam, S. Ahmad, Spectroscopic (FTIR, FT-Raman, <sup>1</sup>H NMR and UV-Vis) and DFT/TD-DFT studies on cholesteno [4,6-b,c]-2',5'-dihydro-1',5'-benzothiazepine, J. Mol. Struct. 1178 (2019) 570-582, <https://doi.org/10.1016/j.molstruc.2018.10.063>
- [19] N.U. Kumar, B.S. Reddy, V. P. Reddy, R. Bandichhor, Zinc triflate catalyzed acylation of alcohols, phenols, and thiophenols, Tetrahedron Lett. 55 (2014) 910-912, <https://doi.org/10.1016/j.tetlet.2013.12.039>
- [20] M.A. Spackman, J.J. McKinnon, Fingerprinting intermolecular interactions in molecular crystals, CrystEngComm 4 (2002) 378-392, <https://doi.org/10.1039/B203191B>
- [21] M.A. Spackman, P.G. Byrom, A novel definition of a molecule in a crystal, Chem. Phys. Lett. 267 (1997) 215-220, [https://doi.org/10.1016/S0009-2614\(97\)00100-0](https://doi.org/10.1016/S0009-2614(97)00100-0)
- [22] J.J. McKinnon, M.A. Spackman, A.S. Mitchell, Novel tools for visualizing and exploring intermolecular interactions in molecular crystals, Acta Cryst. B60 (2004) 627-668, <https://doi.org/10.1107/S0108768104020300>
- [23] S.K. Wolff, D.J. Grimwood, J.J. McKinnon, D. Jayatilaka, M.A. Spackman, CrystalExplorer 2.0, University of Western Australia, Perth, Australia, 2007, <https://crystalexplorer.scb.uwa.edu.au/>
- [24] F.H. Allen, O. Kennard, D.G. Watson, L. Brammer, A.G. Orpen, R.J. Taylor, Tables of bond lengths determined by X-ray and neutron diffraction. Part 1. Bond lengths in organic compounds, Chem. Soc. Perkin Trans. 2 (1987) S1-S19, <https://doi.org/10.1039/P298700000S1>
- [25] H. Khanam, A. Mashrai, N. Siddiqui, M. Ahmad, M.J. Alam, S. Ahmad, Shamsuzzaman, Structural elucidation, density functional calculations and contribution of intermolecular interactions in cholest-4-en-3-one crystals: insights from X-ray and

- hirshfeld surface analysis, *J. Mol. Struct.* 1084 (2015) 274-283, <https://doi.org/10.1016/j.molstruc.2014.12.027>
- [26] M.J. Frisch, G.W. Trucks, H.B. Schlegel, G.E. Scuseria, M.A. Robb, J.R. Cheeseman, G. Scalmani, V. Barone, B. Mennucci, G.A. Petersson, H. Nakatsuji, M. Caricato, X. Li, H.P. Hratchian, A.F. Izmaylov, J. Bloino, G. Zheng, J.L. Sonnenberg, M. Hada, M. Ehara, K. Toyota, R. Fukuda, J. Hasegawa, M. Ishida, T. Nakajima, Y. Honda, O. Kitao, H. Nakai, T. Vreven, J.A. Montgomery Jr., J.E. Peralta, F. Ogliaro, M. Bearpark, J.J. Heyd, E. Brothers, K.N. Kudin, V.N. Staroverov, R. Kobayashi, J. Normand, K. Raghavachari, A. Rendell, J.C. Burant, S.S. Iyengar, J. Tomasi, M. Cossi, N. Rega, J.M. Millam, M. Klene, J.E. Knox, J.B. Cross, V. Bakken, C. Adamo, J. Jaramillo, R. Gomperts, R.E. Stratmann, O. Yazyev, A.J. Austin, R. Cammi, C. Pomelli, J.W. Ochterski, R.L. Martin, K. Morokuma, V.G. Zakrzewski, G.A. Voth, P. Salvador, J.J. Dannenberg, S. Dapprich, A.D. Daniels, Ö. Farkas, J.B. Foresman, J.V. Ortiz, J. Cioslowski, D.J. Fox, *Gaussian 09, Revision D.01*, Gaussian Inc, Wallingford, CT, 2009, <https://gaussian.com/>
- [27] A.D. Becke, Density functional thermochemistry. III. The role of exact exchange, *J. Chem. Phys.* 98 (1993) 5648-5652, <https://doi.org/10.1063/1.464913>
- [28] C. Lee, W. Yang, R.G. Parr, Development of the colle-salvetti correlation-energy formula into a functional of the electron density, *Phys. Rev. B* 37 (1988) 785-789, <https://doi.org/10.1103/PhysRevB.37.785>
- [29] R. Dennington, T. Keith, J. Millam, *GaussView, Ver. 5*, Semichem Inc, Shawnee Mission KS, 2009, <https://gaussian.com/>
- [30] <https://cccbdb.nist.gov/vibscalejust.asp>
- [31] E.D. Glendening, A.E. Reed, J.E. Carpenter, F. Weinhold. *NBO Version 3.1*, 2003, <https://gaussian.com/>
- [32] L.F. Fiesser, M. Fiesser, "*Steroids*", Reinhold Publishing Corporation, New York, 28 (1959).
- [33] H.P. Weber, B.M. Craven, P. Sawzik, R.K. McMullan, Crystal structure and thermal vibrations of cholesteryl acetate from neutron diffraction at 123 and 20 K, *Acta Cryst. B* 47 (1991) 116-127, <https://doi.org/10.1107/S0108768190009739>

- [34] G. Socrates, *Infrared Characteristic Group Frequencies*, third ed., Wiley Interscience Publications, New York, 1980.
- [35] H.L.J. Makin, D.B.Gower, D.N. Kirk, *Steroid analysis*, Springer-Science Business Media, B.V., 1st edition, 1995, Great Britain.
- [36] W.F. Reynolds, R.G. Enriquez, Choosing the best pulse sequences, acquisition parameters, postacquisition processing strategies, and probes for natural product structure elucidation by NMR spectroscopy, *J. Nat. Prod.* 65 (2002) 221-244, <https://doi.org/10.1021/np010444o>
- [37] M. Arivazhagana, R. Meenakshi, Vibrational spectroscopic studies and DFT calculations of 4-bromo-o-xylene, *Spectrochim. Acta Mol. Biomol. Spectrosc.* (2012) 419-430, <https://doi.org/10.1016/j.saa.2012.01.062>
- [38] R.G. Parr, W. Yang, *Density-functional theory of atoms and molecules*, Oxford University Press, New York, 1989.
- [39] R.G. Parr, W.T. Yang, *Density-functional theory of the electronic structure of molecules*, *Annu. Rev. Phys. Chem.* 46 (1995) 701-728, <https://doi.org/10.1146/annurev.pc.46.100195.003413>
- [40] W. Kohn, A.D. Becke, R.G. Parr, *Density functional theory of electronic structure*, *J. Phys. Chem.* 100 (1996) 12974-12980, <https://doi.org/10.1021/jp960669l>
- [41] P. Geerlings, F. De Proft, W. Langenaeker, *Conceptual density functional theory*, *Chem. Rev.* 103 (2003) 1793-1874, <https://doi.org/10.1021/cr990029p>
- [42] P. Geerlings, F. De Proft, *Conceptual DFT: the chemical relevance of higher response functions*, *Phys. Chem. Chem. Phys.* 10 (2008) 3028-3042, <https://doi.org/10.1039/B717671F>
- [43] P.W. Ayers, J.S.M. Anderson, L.J. Bartolotti, *Perturbative perspectives on the chemical reaction prediction problem*, *Int. J. Quantum Chem.* 101 (2005) 520-534, <https://doi.org/10.1002/qua.20307>
- [44] H. Chermette, *Chemical reactivity indexes in density functional theory*, *J. Comput. Chem.* 20 (1999) 129-154, [https://doi.org/10.1002/\(SICI\)1096-987X\(19990115\)20:1<129::AID-JCC13>3.0.CO;2-A](https://doi.org/10.1002/(SICI)1096-987X(19990115)20:1<129::AID-JCC13>3.0.CO;2-A)

- [45] A. Cherkasov, E.N. Muratov, D. Fourches, A. Varnek, I.I. Baskin, M. Cronin, J. Dearden, P. Gramatica, Y.C. Martin, R. Todeschini, V. Consonni, V.E. Kuz'min, R. Cramer, R. Benigni, C. Yang, J. Rathman, L. Terfloth, J. Gasteiger, A. Richard, A. Tropsha, QSAR modeling: where have you been? where are you going to? *J. Med. Chem.* 2014, 57, 12, 4977-5010, <https://doi.org/10.1021/jm4004285>
- [46] M.R. Paillasse, N. Saffon, H. Gornitzka, S. Silvente-Poirot, M. Poirot, P. de Medina, Surprising unreactivity of cholesterol-5,6-epoxides towards nucleophiles, *J. Lipid. Res.* 53 (2012) 718-725, <https://doi.org/10.1194/jlr.M023689>
- [47] Y. Yang, X. Su, S. Pan, M. Zhang, Y. Wang, J. Han, Z. Yang, Crystal growth and calculation of the electronic band structure and density of states of  $\text{Li}_3\text{Cs}_2\text{B}_5\text{O}_{10}$ , *CrystEngComm* 16 (2014) 1978-1984, <https://doi.org/10.1039/C3CE42084A>

**Research Highlights**

- Synthesis of  $3\beta$ -acetoxy cholest-5-ene using zinc triflate  $\text{Zn}(\text{OTf})_2$  as a catalyst
- Characterization by single crystal XRD, spectroscopy and DFT/B3LYP calculations
- Hirshfeld surface analysis of the synthesized compound

Journal Pre-proof

Declaration of Interest Statement: None

Journal Pre-proof